

DOI:10.1002/ejic.201201346

## X-ray Crystallographic and First-Principles Theoretical Studies of $K_2[TcOCl_5]$ and UV/Vis Investigation of the $[TcOCl_5]^{2-}$ and $[TcOCl_4]^-$ Ions

Erik V. Johnstone,<sup>\*[a]</sup> Philippe F. Weck,<sup>[b]</sup> Frederic Poineau,<sup>[a]</sup> Eunja Kim,<sup>[c]</sup> Paul M. Forster,<sup>[a]</sup> Alfred P. Sattelberger,<sup>[a,d]</sup> and Kenneth R. Czerwinski<sup>[a]</sup>

**Keywords:** Technetium / Synthesis design / Density functional calculations / Structure elucidation / Radiopharmaceuticals

Dipotassium pentachloridooxidotechnetate,  $K_2[TcOCl_5]$ , has been isolated as green single crystals by the dissolution of  $(NH_4)TcO_4$  in 12 M HCl at 0 °C and careful precipitation with KCl. The structure of this compound was determined by single-crystal X-ray diffraction analysis [ $a = 13.0815(9)$ ,  $b = 9.8982(6)$ ,  $c = 6.7623(4)$  Å;  $V = 875.605$  Å<sup>3</sup>, orthorhombic,  $Pnma$ ,  $Z = 4$ ] and compared with the corresponding molybdenum and rhenium analogues.

The structure of  $K_2[TcOCl_5]$  was also investigated by density functional theory, and the results are in agreement with the crystallographic data. The oscillator strengths of the electronic transitions in the  $C_{4v}$  complex anions  $[TcOCl_5]^{2-}$  and  $[TcOCl_4]^-$  were also calculated by using time-dependent density functional theory and compared with the experimental UV/Vis spectra.

### Introduction

Pentachloridooxidometallate(V)  $[MOCl_5]^{2-}$  complex anions are formed with the transition metals V, Nb, Ta, Cr, Mo, W, Tc, and Re. They can also be precipitated as crystalline salts with the heavier alkali metals (i.e., K, Rb, and Cs) or other small monocationic counter ions, such as  $NH_4^+$ .<sup>[1–4]</sup> When precipitated as the caesium salt, these compounds crystallize in the cubic lattice with space group  $Fm3m$ , whereas with  $K^+$ ,  $Rb^+$ , or  $NH_4^+$ , the orthorhombic  $Pnma$  structure is observed. Both the cubic and orthorhombic structures are based on close-packing of the  $[MOCl_5]^{2-}$  anions with the cations located in the tetrahedral holes.<sup>[1]</sup> The combination of the strong  $M=O$  interactions and readily exchangeable chlorido ligands makes these six-coordinate compounds important precursors to a variety of polyatomic oxido-containing metal complexes. Technetium ( $Z = 43$ ) is a transition-metal element of particular interest, primarily due to the synergy of its radiolytic properties and

rich coordination chemistry, which has been widely utilized in the field of radiopharmaceuticals.<sup>[5]</sup> Its short half-life ( $t_{1/2} = 6$  h) and energetically favorable  $\gamma$  decay energy ( $E_\gamma = 140$  keV) make the metastable isotope  $^{99m}Tc$  an ideal imaging agent for diagnostic nuclear medicine. Macroscopic manipulations of the pure  $\beta$ -emitting daughter isotope and ground state  $^{99}Tc$  ( $t_{1/2} = 2.1 \times 10^5$  years,  $E_{max} = 0.3$  MeV) allow for a better understanding of the fundamental chemistry of Tc, including structural and physical characterizations of the many inorganic and organometallic complexes used for body and organ imaging. Because  $^{99m}Tc$  is eluted as  $Na^{99m}TcO_4$  in isotope generators that separate technetium from its parent nuclide (i.e.,  $^{99}Mo$ ,  $t_{1/2} = 66$  h) by means of column chromatography, typical syntheses of Tc radiopharmaceuticals start from  $Tc^{VII}$  pertechnetate solutions. These solutions undergo “one-pot” reactions with a specific ligand, reductant, and stabilizer to quickly and easily form low-valent  $^{99m}Tc$  complexes ready for injection.<sup>[6–8]</sup> Two easily synthesized, reduced-oxidation-state species derived from pertechnetate, tetrachloridooxidotechnetate(V),  $[TcOCl_4]^-$ , and pentachloridooxidotechnetate(V),  $[TcOCl_5]^{2-}$ , are useful precursors for the synthesis of other molecules with the  $Tc^V=O$  core.<sup>[9–11]</sup>

The preparation of salts of  $[TcOCl_x]^{n-}$  ( $x = 4, 5$ ;  $n = 1, 2$ ) entails the  $2 e^-$  reduction of  $Tc^{VII}$  in cold concentrated HCl to the  $Tc^V$  intermediates, which must be isolated relatively quickly to prevent further reduction to the thermodynamically very stable octahedral technetium(IV) complex,  $[TcCl_6]^{2-}$ . Solution studies have shown that both  $Tc^V$  species are present in an equilibrium that favors the monoanion {i.e.,  $[TcOCl_4]^- + Cl^- \rightleftharpoons [TcOCl_5]^{2-}$ ,  $k =$

[a] Department of Chemistry, University of Nevada Las Vegas, Las Vegas, NV 89154, USA  
Fax: +1-702-895-1907  
E-mail: Erikjohnstone@gmail.com  
Homepage: <http://radchem.nevada.edu/>

[b] Sandia National Laboratories, Albuquerque, NM 87185, USA

[c] Department of Physics and Astronomy, University of Nevada Las Vegas, Las Vegas, NV 89154, USA

[d] Energy Engineering and Systems Analysis Directorate, Argonne National Laboratory, Argonne, IL 60439, USA

Supporting information for this article is available on the WWW under <http://dx.doi.org/10.1002/ejic.201201346>.

$(1.5 \pm 1.0) \times 10^{-3} \text{ M}^{-1}$  in concentrated HCl at ambient temperature}, but each can be selectively isolated according to the size of the coordinating cation.<sup>[12]</sup> The  $[\text{TcOCl}_4]^-$  anion is isolated by precipitation using a large cation such as  $[\text{Bu}_4\text{N}]^+$ ,  $[(\text{C}_6\text{H}_5)_4\text{As}]^+$ , or  $[(\text{Ph}_3\text{P})_2\text{N}]^+$ . Under the same experimental conditions, six-coordinate  $[\text{TcOCl}_5]^{2-}$  has been isolated by using smaller monocations [i.e.,  $\text{M} = \text{K}^+$ ,  $\text{Cs}^+$ ,  $\text{NH}_4^+$ , or  $\text{N}(\text{CH}_2\text{CH}_3)_4^+$ ].<sup>[12]</sup> These complexes have been characterized by IR and Raman spectroscopy, magnetic measurements, and UV/Vis spectroscopy.<sup>[13–16]</sup> The solid-state structure of  $[(\text{Ph}_3\text{P})_2\text{N}][\text{TcOCl}_4]$  was determined by single-crystal X-ray diffraction (SCXRD), and – although no single crystal data for salts containing the  $[\text{TcOCl}_5]^{2-}$  anion have been reported – the salt  $\text{Cs}_2[\text{TcOCl}_5]$  has been characterized by powder XRD and EXAFS; it crystallizes with a cubic lattice.<sup>[11,12,17]</sup> The primary goal of this study was to isolate single crystals of the potassium salt of  $[\text{TcOCl}_5]^{2-}$  and to characterize its crystal structure by using combined XRD and first-principles theoretical approaches. The spectral properties of the  $[\text{TcOCl}_5]^{2-}$  and  $[\text{TcOCl}_4]^-$  complexes formed upon dissolution of the  $\text{K}_2[\text{TcOCl}_5]$  salt have also been investigated by UV/Vis spectroscopy and time-dependent density functional theory (TD-DFT).

## Results and Discussion

### Crystal Structure of Dipotassium Oxopentachlorotechnetate

Dipotassium pentachloridooxidotechnetate(V) was isolated as green, hexagonal single crystals (Figure 1) by the reduction of  $\text{NH}_4\text{TcO}_4$  in cold concentrated HCl followed by slow precipitation with a solution of HCl saturated with KCl at 0 °C. Single-crystal analysis of  $\text{K}_2[\text{TcOCl}_5]$  (Table 1) reveals a six-coordinate distorted octahedron that crystallizes in the orthorhombic  $Pnma$  space group with  $D_{2h}$  symmetry (IT No. 62) and unit-cell lattice parameters  $a = 13.0815(9)$ ,  $b = 9.8982(6)$ , and  $c = 6.7623(4)$  Å ( $V = 875.605$  Å<sup>3</sup>, final  $R$  factor = 2.52%). The unit-cell parameters calculated by DFT are  $a = 13.55$ ,  $b = 10.16$ , and  $c = 6.98$  Å, slightly larger than the experimentally determined values owing to the well-known tendency of generalized gradient approximation (GGA) functionals to overestimate bond lengths. The computed ratios,  $b/a = 0.75$  and  $c/a = 0.51$ , are, however, in excellent agreement with the XRD ratios,  $b/a = 0.7566$  and  $c/a = 0.5169$ . The  $d^2$  complex is isomorphous with two other early-transition-metal pentachloridooxidometallate salts  $\text{K}_2[\text{MOCl}_5]$  ( $\text{M} = \text{Mo}$ ,  $\text{Re}$ ),<sup>[18,19]</sup> with the “ $\text{K}_2[\text{OsNCl}_5]$  structure type”. In the  $[\text{TcOCl}_5]^{2-}$  anion (Figure 2), the  $\text{Tc}=\text{O}$  bond length is 1.634(3) Å (1.68 Å by DFT), which is similar to that found in other octahedral  $\text{Tc}^{\text{V}}=\text{O}$ -containing compounds. There are two different  $\text{Tc}-\text{Cl}$  linkages located *cis* and *trans* to the central  $\text{Tc}=\text{O}$  bond that are defined within the structure. The bonds of the three equatorial chlorine atoms *cis*  $\text{Tc}-\text{Cl}(3,4,5)$  are significantly shorter [av.  $\text{Tc}-\text{Cl}$  2.3763(7) Å; av.  $\text{Tc}-\text{Cl}$  2.40 Å by DFT] than the *trans*  $\text{Tc}-\text{Cl}$  bond. Of the four Cl atoms occupying the equatorial plane, the two symmetry-equivalent  $\text{Tc}-\text{Cl}(3)$  distances are slightly longer than

$\text{Tc}-\text{Cl}(4)$  and  $\text{Tc}-\text{Cl}(5)$ . In comparison with the  $\text{Tc}-\text{Cl}$  linkages of square-pyramidal  $[\text{TcOCl}_4]^-$  [i.e., av.  $\text{Tc}-\text{Cl}$  2.305(2) Å], those found in  $[\text{TcOCl}_5]^{2-}$  are 0.07(1) Å longer, a phenomenon observed for the  $\text{Tc}-\text{X}$  distances of five- and six-coordinate structures.<sup>[10,17]</sup> Because of the structural *trans* effect (STE) of the oxido ligand, the single axial *trans*  $\text{Tc}-\text{Cl}(2)$  bond [2.5389(9) Å; 2.57 Å by DFT] is significantly longer than those of the basal  $\text{Tc}-\text{Cl}$  linkages. In comparison, the octahedral  $\text{Tc}^{\text{V}}=\text{O}$ -containing complex with the quadridentate Schiff-base ligand  $N,N'$ -propane-1,3-diylbis(salicylideneimine) ( $\text{H}_2\text{salpd}$ ), that is,  $[\text{TcOCl}(\text{salpd})]^0$ , exhibits an axial *trans*  $\text{Tc}-\text{Cl}$  bond length of 2.44 Å, whereas for  $\text{Cs}_2[\text{Tc}^{\text{VI}}\text{NCl}_5]$  the *trans*  $\text{Tc}-\text{Cl}$  bond is 2.740(5) Å long, which demonstrates the increased influence of the opposing axial triple-bonded  $\text{Tc}-\text{N}$  linkage in comparison with  $\text{Tc}=\text{O}$ .<sup>[20,21]</sup> The *trans*  $\text{Tc}-\text{Cl}(2)$  linkage in  $\text{K}_2[\text{TcOCl}_5]$  is one of the longest  $\text{Tc}-\text{Cl}$  bonds that has been reported for compounds with a  $\text{Tc}^{\text{V}}=\text{O}$  core. Evidence for the distortion of the six-coordinate octahedron is seen in the bond angles of 94.9 and 82.4° (95.6 and 82.2° by DFT) for  $\text{O}-\text{Tc}-\text{Cl}(3)$  and  $\text{Cl}(4)-\text{Tc}-\text{Cl}(2)$ , respectively, as well as for the  $\text{O}-\text{Tc}-\text{Cl}(2)$  bond angle, which is slightly less than 180° (i.e., 178.7°; 178.5° by DFT). The distortion displaces the Tc atom slightly above (i.e., 0.248 Å) the equatorial plane of the *cis*-Cl ligands towards the terminal O atom. The magnitude of the displacement is similar to that noted for other octahedral  $(\text{TcO})^{3+}$  core complexes.<sup>[6]</sup> The EXAFS data previously obtained<sup>[12]</sup> for  $\text{Cs}_2[\text{TcOCl}_5]$  and the calculated DFT parameters are in close agreement with the structural parameters determined by SCXRD (cf. Table 2). Atomic coordinates and additional structural parameters derived from XRD (see Table S1) and a polyhedral unit-cell packing diagram (see Figure S2) are provided in the Supporting Information.



Figure 1. Optical microscopy image of a single crystal of  $\text{K}_2[\text{TcOCl}_5]$ .

The structural data for the technetium salt were compared with those of the molybdenum and rhenium analogues (Table 3); the three salts show similar *cis*  $\text{M}-\text{Cl}$  bond lengths. The largest difference between the three salts is observed for the  $\text{M}=\text{O}$  bond and the corresponding relationship with the *trans*  $\text{M}-\text{Cl}$  bond; the stronger the  $\text{M}=\text{O}$  bond, the longer the *trans*  $\text{M}-\text{Cl}$  distance, which is a direct

Table 1. Crystal data and refinement details for  $K_2[TcOCl_5]$ .

Empirical formula	$Cl_5K_2Otc$
$M_r$	369.45
Crystal system	orthorhombic
Space group	$Pnma$
$a$ [Å]	13.0815(9)
$b$ [Å]	9.8982(6)
$c$ [Å]	6.7623(4)
$\alpha = \beta = \gamma$ [°]	90
$V$ [Å <sup>3</sup> ]	875.60(10)
$Z$	4
$\lambda$ [Å]	0.71073
$\mu$ [mm <sup>-1</sup> ] [Mo-K $\alpha$ ]	4.039
$F(000)$	696
$T$ [K]	100(2)
$\theta$ range [°]	3.11–30.51
Independent reflections	1409
Independent reflections with $I \leq [2\sigma(I)]$	1367
Goodness-of-fit ( $F^2$ )	1.129
$R1$	0.0252
$wR2$ [ $I \leq 2\sigma(I)$ ]	0.0793

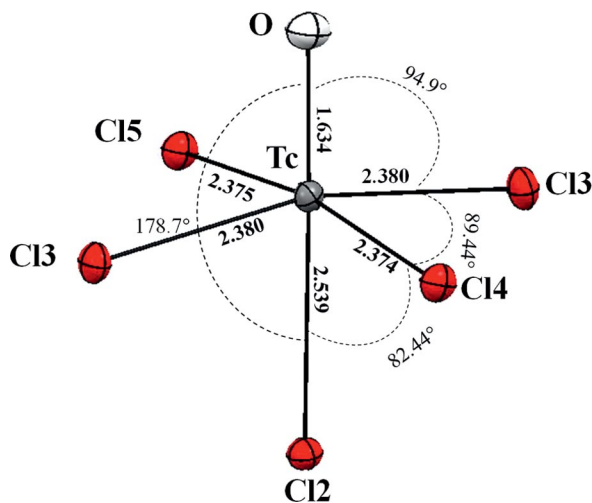


Figure 2. ORTEP representation of the  $[TcOCl_5]^{2-}$  complex composing the  $K_2[TcOCl_5]$  crystal. Distances are in Å and angles in °.

Table 2. Interatomic distances determined by single-crystal X-ray diffraction, EXAFS,<sup>[12]</sup> and DFT for the  $K_2[TcOCl_5]$  crystal.

Method	Tc=O [Å]	av. Tc–Cl <sub>cis</sub> [Å]	Tc–Cl <sub>trans</sub> [Å]
XRD	1.634(3)	2.3763(7)	2.5389(9)
EXAFS <sup>[a]</sup>	1.65	2.36	2.50
DFT	1.68	2.40	2.57

[a] For  $Cs_2[TcOCl_5]$ .

result of the STE. For technetium, the Tc=O distance is slightly longer than that of the molybdenum complex, but about 0.02(1) Å shorter than in the rhenium complex. Transversely, as a result of the STE on the *trans* M–Cl distances, the molybdenum complex exhibits the longest *trans* M–Cl distance (2.59 Å), which is approximately 0.06 and 0.09 Å longer than the technetium and rhenium *trans* M–Cl distances, respectively. The effect of the STE decreases in the order Mo > Tc > Re.

Table 3. Interatomic distances [Å] in the  $K_2[MoOCl_5]$ ,<sup>[18]</sup>  $K_2[TcOCl_5]$ , and  $K_2[ReOCl_5]$ <sup>[21]</sup> crystals determined by single-crystal X-ray diffraction analysis.

Complex	M=O [Å]	av. M–Cl <sub>cis</sub> [Å]	M–Cl <sub>trans</sub> [Å]
$K_2[MoCl_5]$	1.61(1)	2.386(6)	2.587(6)
$K_2[TcOCl_5]$	1.634(3)	2.3763(7)	2.5389(9)
$K_2[ReOCl_5]$	1.655(6)	2.378(6)	2.502(2)

### Molecular Structure and UV/Vis Spectroscopy of $[TcOCl_5]^{2-}$ and $[TcOCl_4]^-$

The dissolution of either  $(nBu_4N)[TcOCl_4]$  or  $K_2[TcOCl_5]$  in 12 M HCl at 0 °C yielded a greenish-yellow solution. The UV/Vis spectra (cf. Figure S1 in the Supporting Information) of these solutions display analogous absorption maxima at around 230, 295, 475, 582, 882, 960, and 1160 nm. The similarities between the two spectra are indicative of the equilibrium formed between the two species in HCl solution (see above).

To assign the bands observed in the UV/Vis spectra, geometry optimization of the  $[TcOCl_5]^{2-}$  and  $[TcOCl_4]^-$  complexes was performed by DFT followed by time-dependent DFT (TD-DFT) calculations of the oscillator strengths and transition energies associated with the relaxed  $[TcOCl_5]^{2-}$  and  $[TcOCl_4]^-$  complexes by using the Gaussian 09 software (details are given in the Supporting Information).<sup>[22]</sup> This approach has been used successfully in previous studies on the speciation of technetium.<sup>[23]</sup>

A study of the structural relaxation of the  $[TcOCl_5]^{2-}$  complex at the GGA/B3LYP (GGA/PBE) level of theory resulted in a  $C_{4v}$  conformer with the following computed bond lengths and angles: Tc–O 1.69 Å (1.70 Å), Tc–Cl3 2.49 Å (2.48 Å), Tc–Cl2 2.51 Å (2.51 Å), Cl3–Tc–Cl4 89.8° (89.8°), Cl2–Tc–Cl3 86.9° (86.7°), Cl3–Tc–Cl3 173.7° (173.3°), O–Tc–Cl2 180.0° (180.0°). These calculated bond lengths and angles compare well with the results obtained with VASP. The structural relaxation of the  $C_{4v}$ -symmetric  $[TcOCl_4]^-$  complex analyzed at the GGA/B3LYP level of theory resulted in the following bond lengths and angles: Tc–O 1.67 Å, Tc–Cl3 2.40 Å, Cl3–Tc–Cl4 85.2°, Cl3–Tc–Cl3 146.5°.

The electronic structures of  $[TcOCl_5]^{2-}$  and  $[TcOCl_4]^-$  reflect the  $C_{4v}$  symmetry of these complexes with doubly degenerate molecular orbitals (MOs) for the E representation and nondegenerate MOs belonging to the  $A_1$ ,  $A_2$ ,  $B_1$ , or  $B_2$  representations of this point group [cf. Figure 3 (top and bottom)]. The HOMO–LUMO energy gaps calculated at the B3LYP/SDD level of theory for  $[TcOCl_5]^{2-}$  and  $[TcOCl_4]^-$  are 2.49 and 2.92 eV, respectively, that is, smaller than the energy gap of  $TcO_4^-$  (5.15 eV), but significantly larger than the gap of the hexahalogenidotechnetate(IV) complexes  $[TcX_6]^{2-}$  (X = Cl, Br; typically ca. 1–1.5 eV).<sup>[24]</sup> Note that the larger HOMO–LUMO gap of  $[TcOCl_4]^-$  compared with  $[TcOCl_5]^{2-}$  suggests a higher chemical stability of this complex.

As shown in Figure 4 (top), the virtual molecular orbitals (MOs) of the  $[TcOCl_5]^{2-}$  complex exhibit predominantly Tc 4d characteristics, except for L+5 and L+6, which have

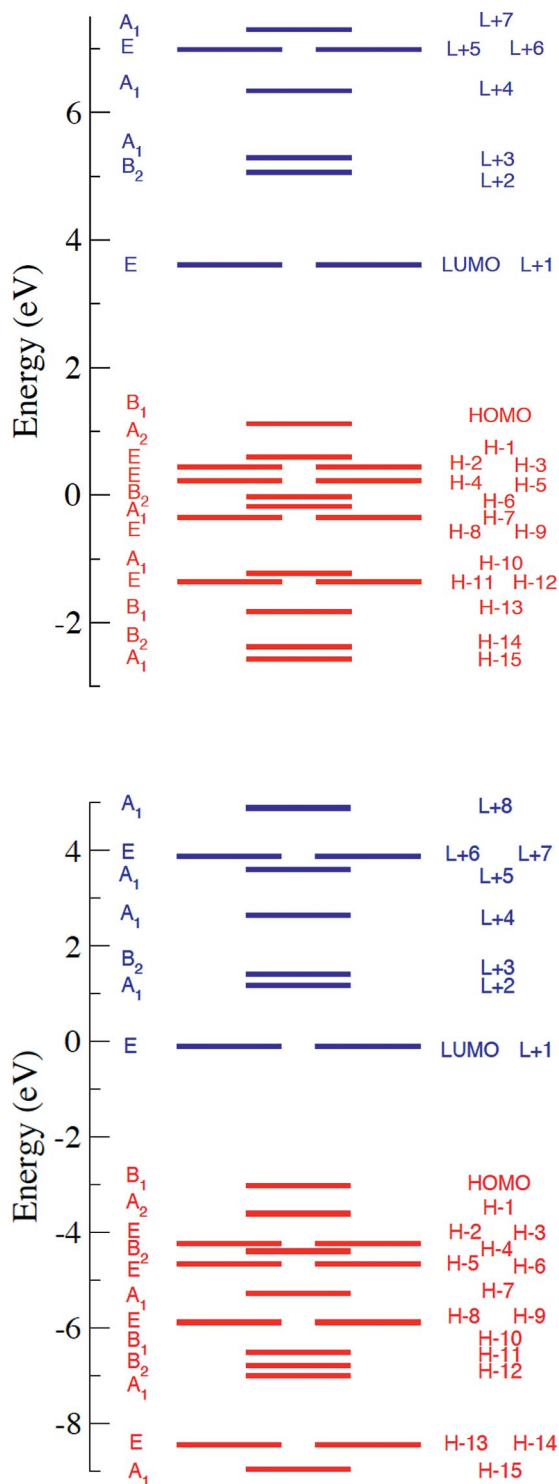


Figure 3. Top: Schematic energy-level diagram of the highest-lying molecular states of the  $C_{4v}$ -symmetric  $[\text{TcOCl}_5]^{2-}$  complex calculated at the B3LYP/SDD level of theory. The lowest unoccupied molecular orbitals (LUMOs) are represented in blue and the highest occupied molecular orbitals (HOMOs) in red. The symmetry of each molecular orbital is indicated on the left. Bottom: Schematic energy-level diagram of the highest-lying molecular states of the  $C_{4v}$ -symmetric  $[\text{TcOCl}_4]^-$  complex calculated at the B3LYP/SDD level of theory. The lowest unoccupied molecular orbitals (LUMOs) are represented in blue and the highest occupied molecular orbitals (HOMOs) in red. The symmetry of each molecular orbital is indicated on the left.

weak Tc 4d character, with some O 2p orbital contributions (LUMO, L+1, and L+3 to L+7) or some degree of Cl 3p character (L+2, L+3, and L+5 to L+7). The HOMO possesses strong Tc  $4d_{xy}$  character with some contribution from the Cl  $3p_{xy}$  orbitals, whereas MOs H-1 to H-10 are essentially ligand-localized, with Cl 3p orbital contributions (H-1 to H-15) and, in some cases, some O 2p character (H-7 to H-12 and H-15). The lower-lying occupied MOs, H-11 to H-15, feature a significant degree of Tc 4d character. This combination of ligand-localized occupied MOs and low-lying unoccupied MOs with marked Tc 4d character points to ligand-to-metal charge transfer (LMCT), that is, O 2p  $\rightarrow$  Tc 4d or Cl 3p  $\rightarrow$  Tc 4d transitions.

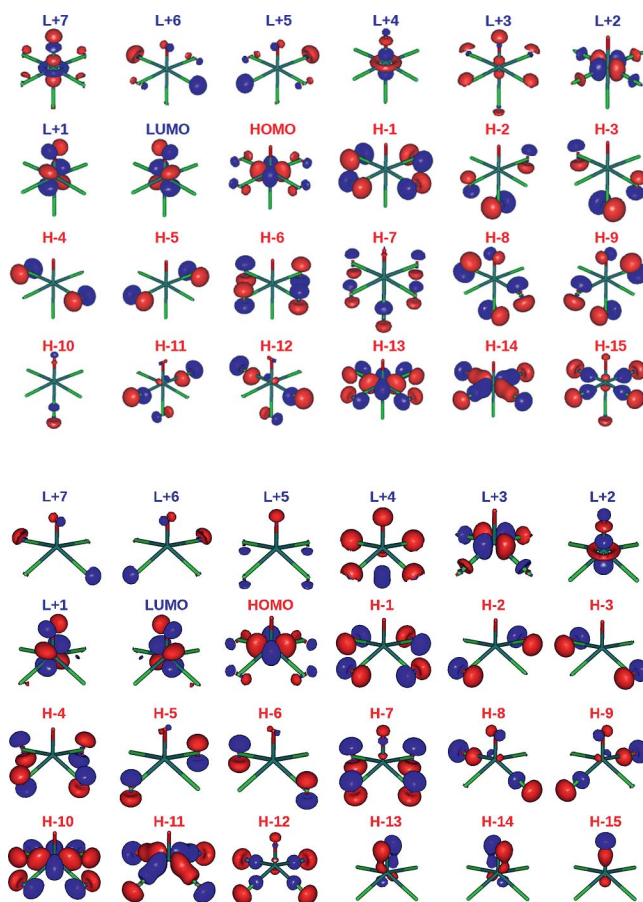


Figure 4. Top: Schematic representation of the highest-lying molecular orbitals of the  $C_{4v}$ -symmetric  $[\text{TcOCl}_5]^{2-}$  complex calculated at the B3LYP/SDD level of theory. Bottom: Schematic representation of the highest-lying molecular orbitals of the  $C_{4v}$ -symmetric  $[\text{TcOCl}_4]^-$  complex calculated at the B3LYP/SDD level of theory. Color code: Tc, dark green; O, red; Cl, light green.

The highest-lying molecular orbitals of the  $[\text{TcOCl}_4]^-$  complex are depicted in Figure 4 (bottom). There is a high degree of similarity between the  $[\text{TcOCl}_4]^-$  MOs and those of the  $[\text{TcOCl}_5]^{2-}$  complex discussed above. Therefore, LMCT transitions are also expected to be dominant between ligand-localized occupied MOs and low-lying unoccupied MOs with marked Tc 4d character.

Oscillator strengths for the  $C_{4v}$ -symmetric  $[\text{TcOCl}_5]^{2-}$  and  $[\text{TcOCl}_4]^-$  complexes calculated with TD-DFT at the B3LYP/SDD level of theory are displayed in Figure 5 along with the experimental UV/Vis spectrum of the species formed upon dissolution of  $\text{K}_2[\text{TcOCl}_5]$  in 12 M HCl at 0 °C. As expected for noncentrosymmetric complexes, numerous electronic transitions are allowed. The experimental absorption maxima at around 230, 295, 475, 582, and 960 nm are overall well reproduced by the positions of the computed oscillator strengths of the  $[\text{TcOCl}_5]^{2-}$  and  $[\text{TcOCl}_4]^-$  complexes. However, there are a few minor discrepancies between the recorded UV/Vis spectrum and the TD-DFT data: The low-intensity absorption bands observed at around 882 and 1160 nm are not reproduced by the calculations, and the computed oscillator strengths at 379 nm for  $[\text{TcOCl}_4]^-$  and 381 nm for  $[\text{TcOCl}_5]^{2-}$  do not appear in the UV/Vis spectrum. The residual discrepancies subsisting between theory and experiment may be ascribed to some extent to slight structural distortions of the anionic complex in experiments compared with the ideal  $C_{4v}$  symmetry used in the calculations and to the absence of explicit treatment of the solvent in the calculations. Complete lists of the transition energies and oscillator strengths for the  $[\text{TcOCl}_5]^{2-}$  and  $[\text{TcOCl}_4]^-$  complexes with  $C_{4v}$  symmetry are given in the Supporting Information (cf. Tables S2 and S3) along with the compositions of individual excitations in terms of major one-electron transitions between the molecular orbital levels schematically represented in Figure 3 (top and bottom, respectively).

At short wavelengths, the most intense oscillator strengths of the  $[\text{TcOCl}_5]^{2-}$  complex are found at 214 nm {intensity: 0.0839; [H-8, H-9]→L+4 (34%), H-1→[L+5, L+6] (32%), [H-2, H-3]→L+7 (20%), [H-11, H-12]→L+2 (10%)}, 221 nm {intensity: 0.0687; H-7→L+4 (86%)}, 222 nm {intensity: 0.0721; [H-8, H-9]→L+3 (38%), [H-8, H-9]→L+4 (30%), [H-11, H-12]→L+2 (20%)}, 234 nm {intensity: 0.0985; H-7→L+3 (92%)}, 243 nm {intensity: 0.0909; [H-4, H-5](E)→L+3 (60%), HOMO→[L+5, L+6] (38%)}, 276 nm {intensity: 0.0326; [H-8, H-9]→L+2 (82%)}, and 293 nm {intensity: 0.0151; [H-11, H-12]→[LUMO, L+1] (84%)}. The oscillator strengths at 234 and 293 nm are in very good agreement with the absorption maxima at 230 and 295 nm, respectively. At longer wavelengths, predicted oscillator strengths are located at 381 nm {intensity: 0.0339; [H-8, H-9]→[LUMO, L+1] (84%)}, 451 nm {intensity: 0.0241; H-7→[LUMO, L+1] (74%)}, 467 nm {intensity: 0.0012; H-6→[LUMO, L+1] (76%)}, 477 nm {intensity: 0.0076; [H-4, H-5]→[LUMO, L+1] (84%)}, 492 nm {intensity: 0.0161; [H-2, H-3]→[LUMO, L+1] (80%)}, and 583 nm {intensity: 0.0002; H-1→[LUMO, L+1] (100%)}. The experimental bands centered at 475 and 582 nm are well reproduced by the oscillator strengths at 477 and 583 nm, respectively.

At short wavelengths, the most intense oscillator strengths of the  $[\text{TcOCl}_4]^-$  complex with  $C_{4v}$  symmetry are located at 220 nm {intensity: 0.0289; H-12→[LUMO, L+1] (72%)}, 250 nm {intensity: 0.0270; [H-5, H-6]→L+2 (36%), [H-5, H-6]→L+3 (28%)}, and 379 nm {intensity:

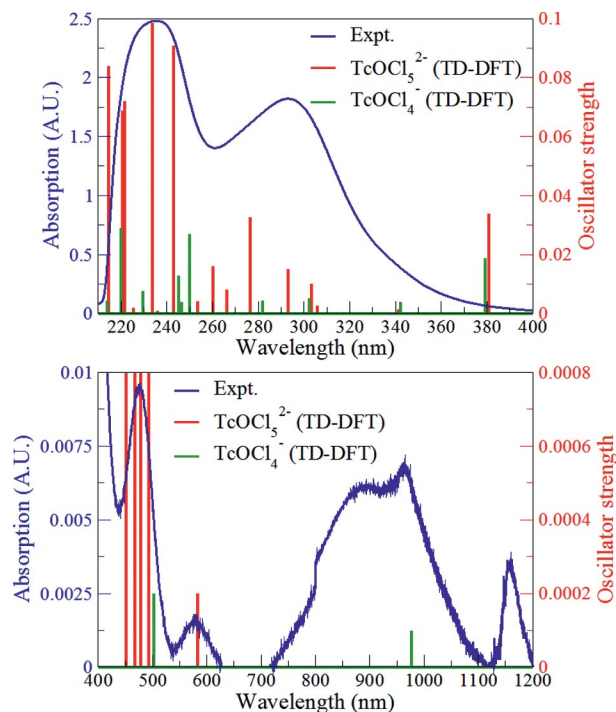


Figure 5. Oscillator strengths for the  $C_{4v}$ -symmetric  $[\text{TcOCl}_5]^{2-}$  and  $[\text{TcOCl}_4]^-$  complexes (red and green vertical bars, respectively) calculated with TD-DFT at the B3LYP/SDD level of theory. The experimental UV/Vis absorption spectrum of  $[\text{TcOCl}_5]^{2-}/[\text{TcOCl}_4]^-$  formed by the dissolution of  $\text{K}_2[\text{TcOCl}_5]$  in 12 M HCl at 0 °C (solid blue line) is superimposed for comparison purpose.

0.0187; H-4→[LUMO, L+1] (98%)}. At longer wavelengths, two transitions of the  $[\text{TcOCl}_4]^-$  complex are predicted at 502 nm {intensity: 0.0002; H-1→[LUMO, L+1] (100%)} and 977 nm {intensity: 0.0001; [HOMO]→[LUMO, L+1] (100%)}. The latter coincides with the absorption maximum observed at 960 nm.

In noncentrosymmetric complexes such as  $[\text{TcOCl}_5]^{2-}$  and  $[\text{TcOCl}_4]^-$  with  $C_{4v}$  point-group symmetry, transitions will be allowed only for certain orientations of the electric vector of the incident light, and pure electronic selection rules might be expected to apply strictly. A detailed analysis of the polarization of the one-electron transitions composing the various bands calculated with TD-DFT is helpful for understanding the UV/Vis spectrum recorded experimentally.

In the  $C_{4v}$  symmetry, the polarization of the following types of allowed transitions needs to be determined: E→E, E→B<sub>2</sub>, E→A<sub>1</sub>, A<sub>1</sub>→A<sub>1</sub>, B<sub>1</sub>→E, A<sub>2</sub>→E, A<sub>1</sub>→E, B<sub>2</sub>→B<sub>2</sub>, and B<sub>2</sub>→E. In the  $C_{4v}$  point group, z belongs to the A<sub>1</sub> representation and x,y to the E representation. The results for the irreducible representations spanned by the dipole integrals  $\int \psi'_z z \psi_e d\tau$  and  $\int \psi'_e(x,y) \psi_e d\tau$  for each of the nine transition types listed above are reported in Table 4. Analysis of these results shows that the only allowed one-electron transitions for z-polarized incident radiation are the E→E, A<sub>1</sub>→A<sub>1</sub>, and B<sub>2</sub>→B<sub>2</sub> transitions, whereas the remaining E→B<sub>2</sub>, E→A<sub>1</sub>, B<sub>1</sub>→E, A<sub>2</sub>→E, A<sub>1</sub>→E, and B<sub>2</sub>→E transitions are only allowed for the x,y-polarized incident radia-

Table 4. Irreducible representations spanned by the dipole integrals  $\int \psi' e z \psi_e d\tau$  and  $\int \psi' e(x,y) \psi_e d\tau$  for the one-electron transitions composing the various bands calculated with TD-DFT.

Transition	$\int \psi' e z \psi_e d\tau$	$\int \psi' e(x,y) \psi_e d\tau$	Polarization of incident radiation	
			$z$	$x,y$
E→E	$A_1+A_2+B_1+B_2$	4E	allowed	forbidden
E→B <sub>2</sub>	E	$A_1+A_2+B_1+B_2$	forbidden	allowed
E→A <sub>1</sub>	E	$A_1+A_2+B_1+B_2$	forbidden	allowed
A <sub>1</sub> →A <sub>1</sub>	A <sub>1</sub>	E	allowed	forbidden
B <sub>1</sub> →E	E	$A_1+A_2+B_1+B_2$	forbidden	allowed
A <sub>2</sub> →E	E	$A_1+A_2+B_1+B_2$	forbidden	allowed
A <sub>1</sub> →E	E	$A_1+A_2+B_1+B_2$	forbidden	allowed
B <sub>2</sub> →B <sub>2</sub>	A <sub>1</sub>	E	allowed	forbidden
B <sub>2</sub> →E	E	$A_1+A_2+B_1+B_2$	forbidden	allowed

tion. This suggests that the optically active  $[\text{TcOCl}_5]^{2-}$  and  $[\text{TcOCl}_4]^-$  complexes will exhibit differing absorption of light polarized along the directions parallel or perpendicular to the  $z$  axis (coinciding with the  $C_4$  axis of the anion), that is, dichroism. This could be verified, for example, by using standard linear dichroism spectroscopic techniques.

From the compositions of the bands calculated for the  $[\text{TcOCl}_5]^{2-}$  complex with TD-DFT (cf. Table S5 in the Supporting Information), it can be seen that only six are composed of pure combinations of allowed one-electron transitions for  $z$ -polarized incident radiation, that is, the bands at 221 nm ( $A_1 \rightarrow A_1$ ; intensity: 0.0687), 234 nm ( $A_1 \rightarrow A_1$ ; intensity: 0.0985), 293 nm (E→E and  $B_2 \rightarrow B_2$ ; intensity: 0.0151), 381 nm (E→E; intensity: 0.0339), 477 nm (E→E; intensity: 0.0076), and 492 nm (E→E; intensity: 0.0161). For the  $[\text{TcOCl}_4]^-$  complex (cf. Table S3 in the Supporting Information), only five computed bands are composed of pure combinations of allowed one-electron transitions for  $z$ -polarized incident radiation: at 214 nm (E→E,  $A_1 \rightarrow A_1$ , and  $B_2 \rightarrow B_2$ ; intensity: 0.0043), 246 nm (E→E and  $A_1 \rightarrow A_1$ ; intensity: 0.0039), 280 nm ( $B_2 \rightarrow B_2$ ; intensity: 0.0003), 342 nm (E→E; intensity: 0.0038), and 388 nm (E→E; intensity: 0.0003). All the other computed bands for the  $[\text{TcOCl}_5]^{2-}$  and  $[\text{TcOCl}_4]^-$  complexes are composed of pure combinations of allowed one-electron transitions for  $x,y$ -polarized incident radiation.

## Conclusions

$\text{K}_2[\text{TcOCl}_5]$  has been isolated and characterized crystallographically and by first-principles theoretical calculations. It is the first single-crystal characterization of the  $[\text{TcOCl}_5]^{2-}$  species. Its structure exhibits an axial  $\text{Tc}=\text{O}$  bond and a correlated elongated *trans*  $\text{Tc}-\text{Cl}$  bond attributed to the STE, as well as four basal Cl atoms in the equatorial plane from which the central Tc atom is vertically displaced. The structure of the Tc complex was compared with those of the isostructural Re and Mo complexes, which showed that the STE decreases in the order  $\text{Mo} > \text{Tc} > \text{Re}$ . The results of the DFT calculations are in agreement with the structural parameters determined by XRD analysis. The MO diagram shows contributions from Tc 4d, Cl 3p, and O 2p orbitals, and the HOMO–LUMO energy gap was determined. Oscillator strengths were calculated with

TD-DFT and correlated with the absorption peaks in the experimental UV/Vis spectrum. To date,  $\text{K}_2[\text{TcOCl}_5]$  is the only  $\text{K}_2[\text{TcOX}_5]$  complex that has been reported crystallographically by using SCXRD. Therefore, it would be of interest to isolate and study the other  $[\text{TcOX}_5]^{2-}$  ( $X = \text{F}, \text{Br}, \text{I}$ ) complexes and compare these with the Cl complex. In addition, because of the popularity of the five-coordinate  $[\text{TcOCl}_4]^-$  as a precursor for radiopharmaceuticals containing the  $(\text{TcO})^{3+}$  core, and structural differences and behavior,  $\text{K}_2[\text{TcOCl}_5]$  serves as a similar but different potential starting material for radiopharmaceuticals.

## Experimental Section

**CAUTION!** Technetium-99 is a weak  $\beta$  emitter ( $E_{\text{max}} = 292$  keV). All manipulations were performed in a laboratory designed for work with radionuclides by using efficient HEPA-filtered fume hoods, Schlenk and glove-box techniques, and applying locally approved radiochemistry handling and monitoring procedures. Laboratory coats, disposable gloves, and protective eyewear were worn at all times.

**Reagents:** Technetium was purchased from Oak Ridge National Laboratory as  $\text{NH}_4\text{TcO}_4$  and used as received. All other reagents were purchased from Sigma–Aldrich and used as received.

**Preparation of Dipotassium Pentachloridooxidotechnetate(V):**  $\text{NH}_4\text{TcO}_4$  (50.6 mg, 0.280 mmol) was placed in a glass scintillation vial, and cold (0 °C) 12 M HCl (3 mL) was added. The vial was capped and lightly agitated for 10 min during which time the flask was periodically vented of the  $\text{Cl}_2$  gas formed. After the reaction, all of the solids had dissolved to yield a dark-green solution. A saturated solution of KCl (450 mg) in 12 M HCl (3 mL) was layered on top of the green liquid and placed in a freezer at  $-23$  °C for single-crystal growth. After approximately 24 h, small, transparent green hexagonal crystals crystallized from the solution (ca. 3 mg). The identity of the compound was confirmed by UV/Vis spectroscopy (see Figure S1 in the Supporting Information).

**Single-Crystal X-ray Diffraction Analysis:** Data were collected with a Bruker Apex II system equipped with an Oxford nitrogen cryostream operating at 100 K. Crystals were mounted under Paratone on a glass fiber. Data processing was performed by using the Apex II suite and an absorption correction applied with SADABS.<sup>[25]</sup> Structure determination (direct methods) and refinement were carried out by using SHELX97 and Olex2.<sup>[26,27]</sup> Further details of the crystal structure investigation may be obtained from the Fachinformationszentrum Karlsruhe, 76344 Eggenstein-Leopoldshafen, Ger-

many (fax: +49-7247-808-666; e-mail: crysdata@fiz-karlsruhe.de), on quoting the depository number CSD-425683.

**Crystal Structure from First-Principle Calculations:** First-principles total energy calculations for the  $K_2[TeOCl_5]$  crystal were performed by using spin-polarized density functional theory (DFT) as implemented in the Vienna ab initio simulation package (VASP).<sup>[28]</sup> The exchange-correlation energy was calculated by using the generalized gradient approximation (GGA) with Perdew–Burke–Ernzerhof (PBE) parametrization.<sup>[29]</sup> Pure functionals, such as the PBE or Perdew–Wang<sup>[30]</sup> (PW91) functionals, have been found in previous studies to correctly describe the geometric parameters and properties of various technetium halide crystals observed experimentally.<sup>[31–34]</sup>

The interaction between valence electrons and ionic cores was described by the projector-augmented wave (PAW) method.<sup>[35,36]</sup> Te  $4p^65s^24d^5$ , K  $3p^64s^1$ , Cl  $3s^23p^5$ , and O  $2s^22p^4$  electrons were treated explicitly as valence electrons in the Kohn–Sham (KS) equations, and the remaining core electrons together with the nuclei were represented by PAW pseudopotentials. The KS equations were solved by using the special blocked Davidson iterative matrix diagonalization scheme.<sup>[37]</sup> The plane-wave cutoff energy for the electronic wavefunctions was set to a value of 500 eV, ensuring the total energy of the system to be converged to within 1 meV/atom. Partial occupancies were set for each wavefunction by using the tetrahedron method with Blöchl corrections.<sup>[38]</sup>

Ionic relaxation was carried out by using the conjugate gradient algorithm and the Hellmann–Feynman forces acting on atoms were calculated with a convergence tolerance set to 0.01 eV/Å. A periodic unit cell approach was used in the calculations. In structural relaxation calculations, the structure determined by XRD was used as the starting geometry, and no symmetry constraints were applied during relaxation. The Brillouin zone was sampled by using the Monkhorst–Pack  $k$ -point scheme<sup>[39]</sup> with a  $k$ -point mesh of  $3 \times 5 \times 5$ .

**Other Techniques:** UV/Vis spectra were recorded at room temperature in a quartz cell (1 cm) with a Cary 6000i double-beam spectrometer. Concentrated HCl was used as the reference. In addition, to assign the spectral signatures observed in the recorded UV/Vis spectrum, DFT calculations of the structural optimization of the  $[TeOCl_5]^{2-}$  anion followed by TD-DFT calculations of the oscillator strengths and transition energies associated with the relaxed complex were carried out by using the Becke 3-parameter, Lee–Yang–Parr<sup>[40–43]</sup> (B3LYP) hybrid functional, the Dunning–Huzinaga valence double-zeta basis set<sup>[44]</sup> (D95V), and the Stuttgart/Dresden effective core potentials<sup>[45]</sup> (SDD) with the Gaussian 09<sup>[22]</sup> software (details of the calculations are provided in the Supporting Information).

**Supporting Information** (see footnote on the first page of this article): Computational method, transition energies, and oscillator strengths for the  $[TeOCl_5]^{2-}$  anion computed with TD-DFT.

## Acknowledgments

The authors would like to thank Julie Bertoia and Trevor Low for outstanding laboratory management and health physics support. Funding for this project was supported by the Department of Energy under the SISGR-Fundamental Chemistry of Technetium-99 Incorporated into Metal Oxide, Phosphate and Sulfide: Toward Stabilization of Low-Valent Technetium (Contract No. 47824B) and the U.S. Department of Energy Award (No. DE-SC00052). Sandia National Laboratories is a multi-program laboratory man-

aged and operated by Sandia Corporation, a wholly owned subsidiary of Lockheed Martin Corporation, for the U.S. Department of Energy's National Nuclear Security Administration under contract DE-AC04-94AL85000.

- [1] J. E. Fergusson, A. M. Greenway, B. R. Penfold, *Inorg. Chim. Acta* **1983**, *71*, 29–34.
- [2] W. F. Jackob, B. Z. Jezowska, *Z. Anorg. Chem.* **1933**, *214*, 337.
- [3] D. J. Brown, *J. Chem. Soc.* **1964**, 4944.
- [4] D. A. Edwards, R. T. Ward, *J. Mol. Struct.* **1970**, *6*, 421.
- [5] B. Johannsen, H. Spies, *Top. Curr. Chem.* **1996**, *176*, 77.
- [6] K. Schwochau in *Technetium: Chemistry and Radiopharmaceutical Applications*, Wiley-VCH, Weinheim, **2000**, pp. 165–380.
- [7] U. Abram, R. Alberto, *J. Braz. Chem. Soc.* **2006**, *17*, 1486.
- [8] H. Braband, *Chimia* **2011**, *65*, 776.
- [9] A. Davison, A. G. Jones, *Int. J. Appl. Radiat. Isot.* **1982**, *33*, 875.
- [10] G. Bandoli, U. Mazzi, E. Roncari, E. Deutsch, *Coord. Chem. Rev.* **1982**, *44*, 191.
- [11] R. W. Thomas, A. Davison, H. S. Trop, E. Deutsch, *Inorg. Chem.* **1980**, *19*, 2840.
- [12] R. W. Thomas, M. J. Heeg, R. C. Elder, E. Deutsch, *Inorg. Chem.* **1985**, *24*, 1472.
- [13] B. Jezowska-Trzebiatowska, S. Wajda, M. Baluka, *Zh. Strukt. Khim.* **1967**, *8*, 524.
- [14] M. Baluka, J. Hanuza, B. Jezowska-Trzebiatowska, *Bull. Acad. Polon. Sci.* **1972**, *20*, 271.
- [15] J. Hanuza, M. Baluka, B. Jezowska-Trzebiatowska, *Acta Phys. Polon.* **1987**, *A71*, 91.
- [16] B. Jezowska-Trzebiatowska, M. Baluka, *Bull. Acad. Polon. Sci.* **1975**, *13*, 1.
- [17] F. A. Cotton, A. Davison, V. W. Day, L. D. Gage, H. Trop, *Inorg. Chem.* **1979**, *18*, 3024.
- [18] V. V. Tkachev, O. N. Krasochka, L. O. Atovmyan, *Zh. Strukt. Khim.* **1976**, *17*, 940.
- [19] T. Glowiak, B. Jezowska-Trzebiatowska, T. Lis, *Acta Crystallogr., Sect. C* **1991**, *47*, 177.
- [20] J. Baldas, S. F. Colmanet, *Inorg. Chim. Acta* **1991**, *179*, 189.
- [21] G. Bandoli, M. Nicolini, U. Mazzi, F. Refosco, *J. Chem. Soc., Dalton Trans.* **1984**, 2505.
- [22] M. J. Frisch, G. W. Trucks, H. B. Schlegel, G. E. Scuseria, M. A. Robb, J. R. Cheeseman, G. Scalmani, V. Barone, B. Mennucci, G. A. Petersson, H. Nakatsuji, M. Caricato, X. Li, H. P. Hratchian, A. F. Izmaylov, J. Bloino, G. Zheng, J. L. Sonnenberg, M. Hada, M. Ehara, K. Toyota, R. Fukuda, J. Hasegawa, M. Ishida, T. Nakajima, Y. Honda, O. Kitao, H. Nakai, T. Vreven, J. A. Montgomery, Jr., J. E. Peralta, F. Ogliaro, M. Bearpark, J. J. Heyd, E. Brothers, K. N. Kudin, V. N. Staroverov, R. Kobayashi, J. Normand, K. Raghavachari, A. Rendell, J. C. Burant, S. S. Iyengar, J. Tomasi, M. Cossi, N. Rega, J. M. Millam, M. Klene, J. E. Knox, J. B. Cross, V. Bakken, C. Adamo, J. Jaramillo, R. Gomperts, R. E. Stratmann, O. Yazyev, A. J. Austin, R. Cammi, C. Pomelli, J. W. Ochterski, R. L. Martin, K. Morokuma, V. G. Zakrzewski, G. A. Voth, P. Salvador, J. J. Dannenberg, S. Dapprich, A. D. Daniels, O. Farkas, J. B. Foresman, J. V. Ortiz, J. Cioslowski, D. J. Fox, *Gaussian 09*, Revision A.02, Gaussian, Inc., Wallingford, CT, **2009**.
- [23] F. Poineau, P. F. Weck, K. German, A. Maruk, G. Kirakosyan, W. W. Lukens, D. B. Rego, A. P. Sattelberger, K. R. Czerwinski, *Dalton Trans.* **2010**, *39*, 8616.
- [24] P. F. Weck, E. Kim, K. R. Czerwinski, *Chem. Phys. Lett.* **2010**, *487*, 190.
- [25] Bruker, *SADABS*, Bruker AXS Inc., Madison, Wisconsin, USA, **2001**.
- [26] G. M. Sheldrick, *Acta Crystallogr., Sect. A* **2008**, *64*, 112.
- [27] O. V. Dolmanov, R. J. Gildea, J. A. K. Howard, H. Puschmann, *J. Appl. Crystallogr.* **2009**, *42*, 339.
- [28] G. Kresse, J. Furthmüller, *Phys. Rev. B* **1996**, *54*, 11169.
- [29] P. Perdew, K. Burke, M. Ernzerhof, *Phys. Rev. Lett.* **1996**, *77*, 3865.

- [30] J. P. Perdew, Y. Wang, *Phys. Rev. B* **1992**, *45*, 13244.
- [31] F. Poineau, E. Johnstone, P. F. Weck, P. M. Forster, E. Kim, K. R. Czerwinski, A. P. Sattelberger, *Inorg. Chem.* **2012**, *51*, 4915.
- [32] F. Poineau, C. D. Malliakas, P. F. Weck, B. L. Scott, E. V. Johnstone, P. M. Forster, E. Kim, M. G. Kanatzidis, K. R. Czerwinski, A. P. Sattelberger, *J. Am. Chem. Soc.* **2011**, *133*, 8814.
- [33] F. Poineau, E. V. Johnstone, P. F. Weck, E. Kim, P. M. Forster, B. L. Scott, A. P. Sattelberger, K. R. Czerwinski, *J. Am. Chem. Soc.* **2010**, *132*, 15864.
- [34] P. F. Weck, E. Kim, F. Poineau, E. Rodriguez, A. P. Sattelberger, K. R. Czerwinski, *Inorg. Chem.* **2009**, *48*, 6555.
- [35] P. E. Blöchl, *Phys. Rev. B* **1994**, *50*, 17953.
- [36] G. Kresse, D. Joubert, *Phys. Rev. B* **1999**, *59*, 1758.
- [37] E. R. Davidson in *Methods in Computational Molecular Physics* (Eds.: G. H. F. Diercksen, S. Wilson), Reidel Publishing Company, Dordrecht, **1983**, vol. 113, p. 95.
- [38] P. E. Blöchl, O. Jepsen, O. K. Andersen, *Phys. Rev. B* **1994**, *49*, 16223.
- [39] H. J. Monkhorst, J. D. Pack, *Phys. Rev. B* **1976**, *13*, 5188.
- [40] A. D. Becke, *J. Chem. Phys.* **1993**, *98*, 5648.
- [41] C. Lee, W. Yang, R. G. Parr, *Phys. Rev. B* **1988**, *37*, 785.
- [42] S. H. Vosko, L. Wilk, M. Nusair, *Can. J. Phys.* **1980**, *58*, 1200.
- [43] P. J. Stephens, F. J. Devlin, C. F. Chabalowski, M. J. Frisch, *J. Phys. Chem.* **1994**, *98*, 11623.
- [44] T. H. Dunning Jr., P. J. Hay in *Modern Theoretical Chemistry* (Ed.: H. F. Schaefer III), Plenum Press, New York, **1976**, vol. 3, pp. 1–28.
- [45] D. Andrae, U. Haeussermann, M. Dolg, H. Stoll, H. Preuss, *Theor. Chem. Acc.* **1990**, *77*, 123.

Received: November 9, 2012

Published Online: January 23, 2013